

# Structural features in the thermopower of a two-dimensional electron gas near topological transitions

N. V. Zavaritskii and I. M. Suslov

*Institute of Physical Problems, Academy of Sciences of the USSR*

(Submitted 24 May 1984)

Zh. Eksp. Teor. Fiz. **87**, 2152–2165 (December 1984)

Transitions associated with changes in the topology of the Fermi surface in two-dimensional (2D) metal systems have been studied theoretically and experimentally. The thermopower  $\alpha$  in inversion layers at a silicon surface, near the (100) plane, has been studied experimentally. The plot of  $\alpha$  versus the surface electron density  $N_S$  (or the Fermi level  $\epsilon_F$ ) is complicated, with abrupt singularities of the order of the observed effect. Near these features, the behavior of  $\alpha$  is described by  $\alpha \propto \Delta\epsilon^{-0.7 \pm 0.3}$  and  $\alpha \propto \Delta\epsilon^{-0.5 \pm 0.3}$ , where  $\Delta\epsilon = \epsilon_F - \epsilon_c$ , for two types of singularities related to (a) the appearance of a neck and (b) the nucleation of a cavity. For the diffuse part of the thermopower,  $\alpha_e$ , and for the thermopower due to phonon drag,  $\alpha_{ph}$ , the following expressions are derived theoretically:  $\alpha_e \propto \Delta\epsilon^{-1}$  and  $\alpha_{ph} \propto |\Delta\epsilon|^{-1/2}$  in case (a) and  $\alpha_e \propto \delta(\Delta\epsilon)$  and  $\alpha_{ph} \propto \Delta\epsilon^{-1/2} \Theta(\Delta\epsilon)$  in case (b). The temperature dependence of  $\alpha$  near the singularities and the nature of the blurring of the singularities is studied. On the whole, the theoretical predictions agree reasonably well with experiment.

## 1. INTRODUCTION

The concept of topological transitions in metals was introduced in 1960 by I. M. Lifshitz.<sup>1</sup> These transitions are associated with changes in the topology of the Fermi surface, which can occur in one of two ways: through the appearance (or rupture) of a neck between two parts of the Fermi surface, or through the onset (or disappearance) of a new cavity. The point of the topological transition is a singularity of both the thermodynamic and kinetic characteristics.<sup>1,2</sup>

A three-dimensional (3D) system is difficult to study experimentally, however, since in such a system it is difficult to attain the large change in electron density which is required for the occurrence of a transition. Such changes have actually been produced only by greatly deforming test samples at high pressures or by introducing a large amount of an impurity.<sup>3–6</sup>

In the two-dimensional (2D) case there are systems in which the electron density can be changed easily during an experiment: the so-called metal-insulator-semiconductor systems.<sup>7</sup> They consist of a metal electrode (the gate) separated from a bulk semiconductor by a thin insulating film. By applying a voltage  $V_g$  between the gate and the interior of the semiconductor, one can create a 2D electron gas with a surface density  $N_S$  which depends on  $V_g$  in a thin surface layer ( $d \sim 50 \text{ \AA}$ ).

A topological transition can be arranged at comparatively low densities  $N_S$  by using metal-insulator-semiconductor structures on superlattices: systems in which an additional spatial periodicity with a period large in comparison with interatomic distances, has been created. In the experiments described below, this additional periodicity arose from the use of surfaces of a silicon crystal with high Miller indices. The sequential changes in the Fermi surface which occur in these systems upon a gradual increase in the density  $N_S$  are shown in Fig. 1. We see that both types of topological transitions mentioned above occur here: the formation of a neck (A) and the onset of a cavity (B). The transitions are

separated because of the minigap  $\Delta$  in the spectrum.

The singularities in the electrical conductivity of 2D systems which result from topological transitions were first observed by Cole *et al.*<sup>8</sup> and were found to be very weak. Recently, some considerably stronger singularities (changes on the order of the effect itself) have been observed in the thermopower  $\alpha$  (Ref. 9). In the present paper we report the results of a more detailed experimental study of the thermopower in metal-insulator-semiconductor structures near to-

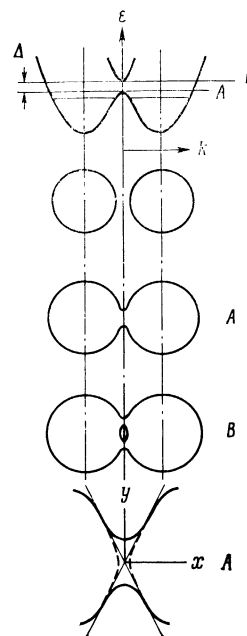


FIG. 1. The electron spectrum  $\epsilon(\mathbf{k})$  for metal-insulator-semiconductor structures on high-index silicon planes. Shown at the left are the sequential changes in the Fermi surface as the density  $N_S$  is increased; the letters specify the topological transitions. A—Appearance of a neck (shown at the bottom in larger scale); B—appearance of a cavity. Dashed line) Boundary of the Brillouin zone; dot-dashed line) centers of electron valleys.

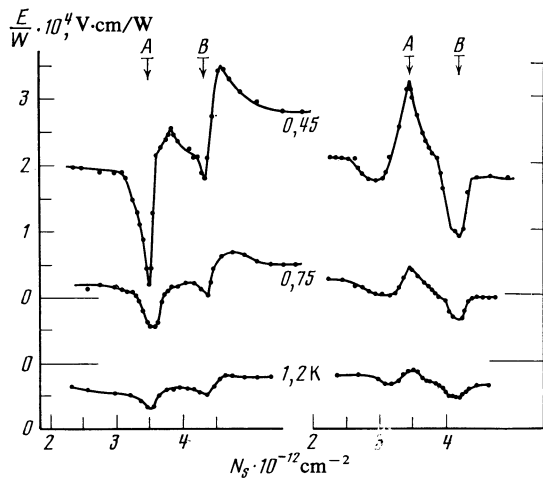


FIG. 2. Thermopower of 2D electron systems in metal-insulator-semiconductor structures on high-index silicon planes. For this sample, the tilt from the (100) plane is  $\theta = 10^\circ 30'$ . The curves at the left correspond to the case in which the heat flux is directed along the superlattice, and those at the right correspond to a heat flux perpendicular to the superlattice. The ordinate scales are successively shifted.

ological transitions in the temperature interval between 0.45 and 2 K, for various directions of the heat flux with respect to the superlattice (Fig. 2). We will compare the experimental data with a theoretical analysis of the singularities in the thermopower of a 2D metal at the points of topological transitions.

## 2. EXPERIMENTAL PROCEDURE

The thermopower  $\alpha$  determines the electric field  $E$  which arises in a sample in which there is a temperature gradient  $\nabla T$  but no electric current  $j$ :

$$E_i = \alpha_{ik} (\nabla T)_k, \quad j = 0.$$

The thermopower can usually be represented as consisting of a diffuse component  $\alpha_e$  and a component due to the phonon drag of electrons,  $\alpha_{ph}$  (Ref. 10):

$$\alpha = \alpha_e + \alpha_{ph} = aT + bT^3. \quad (1)$$

The apparatus shown in Fig. 3 was used to measure the thermopower. The test samples were metal-insulator-semiconductor structures fabricated by the standard procedure on silicon planes making angles  $\theta = 9^\circ, 9^\circ 27', 10^\circ, 10^\circ 30',$  and  $10^\circ 40'$  with the (100) plane; in this case, a superlattice arises in the 2D system along the direction of the tilt. We measured the characteristics of the samples both along and across the superlattice.

The dimensions of these metal-insulator-semiconductor structures were  $400 \times 1200 \mu\text{m}$ . The structures were on silicon wafers  $0.3 \times 3 \times 10 \text{ mm}$  in size. A wire heater  $H_1$  was wound around one end of the wafer, while the other end of the wafer was soldered with indium (2) to a heat sink 3, which was in contact with a  $\text{He}^3$  bath 5 through a germanium insulating washer 4. Heater  $H_2$  was used to change the average temperature of the sample, which was measured with thermometer  $T$ . All these parts of the apparatus were inside a vacuum container 6.

For the measurements of  $E$ , Pb-Sn superconducting

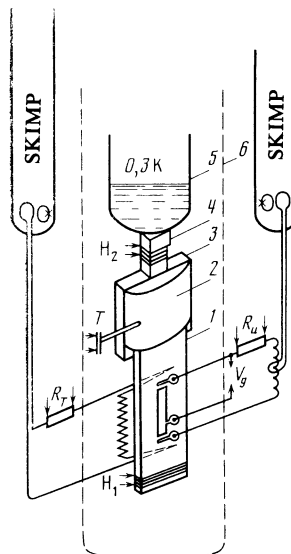


FIG. 3. Apparatus used to study the thermopower in the inversion layers in metal-insulator-semiconductor structures.

leads  $50 \mu\text{m}$  in diameter were soldered to the source and the drain. For the measurements of  $\nabla T$ , the tips of a thermocouple of a superconductor and of ZLZh alloy were cemented to the side of the silicon wafer opposite the metal-insulator-semiconductor structure. The superconducting parts were connected to the apparatus outside the chamber by platinum capillaries sealed in glass beads (not shown in Fig. 3).

The voltages across the sample and the thermocouple were measured by bridge methods, with a SKIMP apparatus<sup>11</sup> used as null detector. An air-core transformer was used in the circuit for measuring the voltage across the metal-insulator-semiconductor structure. This transformer improved the current sensitivity of the apparatus to  $10^{-13}$ – $10^{-14}$  A.

Most of the measurements were taken in the temperature interval 0.45–1.2 K. We measured the conductivity  $\sigma$ , the thermopower  $\alpha$ , and the thermal conductivity  $\kappa$  of the samples. Because of the small geometric size of the samples, the systematic error in the determination of the absolute values of  $\alpha$  or  $\kappa$  could reach 20%. We therefore compared quantities characterizing the relative changes in these properties. For example, instead of the thermopower we used the ratio  $E/W$ , where  $W$  is the heat flux density in the interior of the sample corresponding to the temperature gradient  $\nabla T$  along the structure. The value of  $\nabla T$  along the sample and the metal-insulator-semiconductor structure was  $\nabla T = W/\kappa$ , and the value of  $E/W$  is directly proportional to the thermopower  $\alpha$ . According to the experimental results,  $\kappa$  does not depend on the state of the electron system; we find  $\kappa \approx 2 \cdot 10^{-2} T^3 \text{ W}/(\text{K} \cdot \text{cm})$  in the interval 0.8–4 K and  $\kappa \sim T^{2.6}$  at  $T \leq 0.8$  K. The thermal conductivity is due to phonons, which are scattered primarily by the boundaries of the silicon wafer.

For the study of  $\alpha$  we selected samples for which the leakage current through the  $\text{SiO}_2$  insulating layer was  $< 10^{-12}$ – $10^{-13}$  A over the entire range of gate voltages  $V_g$  used. If we had not selected such samples, it would have been

necessary to take further precautions to maintain a constant sample temperature when heater  $H_1$  was turned on and produced a heat flux  $W$  along the sample. In the experiments, we determined the behavior of  $E/W$  as a function of the density of surface electrons in point-by-point measurements.<sup>1)</sup> The density  $N_S$  was calculated from

$$N_S = C(V_g - V_0)/|e|,$$

where  $e$  is the electron charge,  $C$  is the specific capacitance of the structure, and  $V_0$  is the threshold voltage (these properties were determined in an independent experiment at 80 K). For each of the samples, the measurements were carried out in succession at several temperatures.

Figure 2 shows a typical family of curves of  $E/W$  versus  $N_S$  for metal-insulator-semiconductor structures with  $\theta = 10^\circ 30'$ . The curves at the left correspond to a heat flux directed along the superlattice, while those at the right correspond to the heat flux directed across the superlattice. All of the curves have several sharp peaks, the largest of which we have labeled  $A$  and  $B$ . The shape of these peaks depends on the direction of the heat flux: When the heat flux is directed along the superlattice, there is a minimum value of  $\alpha$  at  $A$ , while for the heat flux in the perpendicular direction  $\alpha$  reaches a maximum here. Regardless of the direction of the heat flux, features  $A$  and  $B$  occur at the same values  $N_A$  and  $N_B$  (Fig. 4).

The absolute heights of peaks  $A$  and  $B$ ,  $\Delta(E/W)$ , can be determined only within an error of up to 10-20% from the  $N_S$  dependence of  $E/W$ . More-reliable information on the height of peak  $A$  can be found in terms of half the difference  $\alpha_\perp^A - \alpha_\parallel^A$ . Figure 5 shows values of  $\Delta(E/W)$  found by the different methods. We see that the absolute height of the peaks increases sharply as the temperature decreases, roughly in proportion to  $T^{-1.6}$ .

To distinguish the diffuse and phonon-drag components of the thermal power, it is convenient to examine the  $T^2$  dependence of  $\alpha/T$  [see expression (1) and Fig. 6]. This behavior must of course be analyzed far from the peaks. We find that at  $T \leq 1.5$  K the thermal power can be described by  $\alpha/T = a + bT^2$ , which follows directly from expression<sup>2)</sup> (1). At higher temperatures we see that  $\alpha/T$  increases much more rapidly with the temperature. The same behavior of the

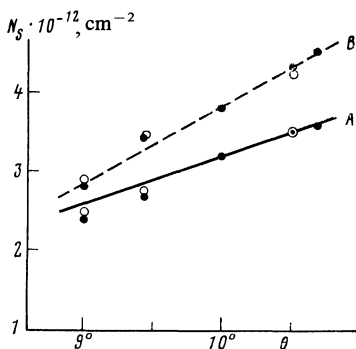


FIG. 4. Critical densities  $N_A$  and  $N_B$  for samples with various angles  $\theta$ . Filled and open circles—Measurements with a heat flux respectively along and across the superlattice; solid line—curve corresponding to  $k_F = 0.15(2\pi/a)\sin\theta$ .

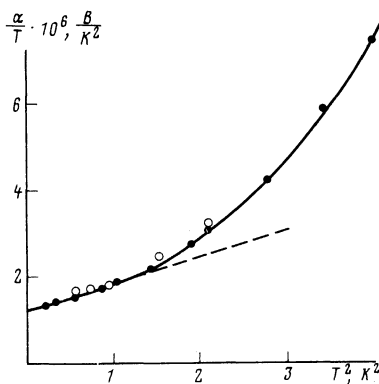


FIG. 5. Temperature dependence of peak  $A$  for samples with various angles  $\theta$ :  $\triangle$ — $9^\circ$ ;  $\circ$ — $9^\circ 27'$ ;  $\bullet$ — $10^\circ 30'$ .

thermal power was observed in Ref. 12 and was attributed there to a significant maximum in  $\alpha_{ph}$  in the 2D electron gas at  $q_T = 2k_F$ , where  $q_T$  is the phonon wave vector corresponding to the maximum of the phonon thermal distribution, and  $\hbar k_F$  is the electron Fermi momentum.

These results show that in analyzing the peaks on the curves of  $E/W$  versus  $N_S$  we must take into account the changes in both the diffuse and phonon components of the thermopower at the topological transitions.

On the conductivity curves  $\sigma(N_S)$  between  $A$  and  $B$  we see  $W$ -shaped peaks with an amplitude of 3-5% of  $\sigma_{reg}$ , similar to those which have been described previously.<sup>7,8</sup> The height and shape of these peaks do not change as the sample is cooled to 0.4 K. For most of the samples the mobility  $\mu_{max}$  is  $\approx 10^4$  cm<sup>2</sup>/(V.s); only for the samples with  $\theta = 9^\circ 27'$  does it reach  $1.9 \cdot 10^4$  cm<sup>2</sup>/(V.s).

### 3. THEORETICAL ANALYSIS OF THE PEAKS IN THE THERMOPOWER

The peaks of  $\alpha_e$  and  $\alpha_{ph}$  [see (1)] differ in nature and must be analyzed separately.

1. *Peak of  $\alpha_e$ .* The diffuse component of the thermopower,  $\alpha_e$ , can be analyzed through a trivial generalization of the theory of Ref. 13 for the 3D case. For  $\alpha_e$  we can use the Mott formula<sup>10</sup>

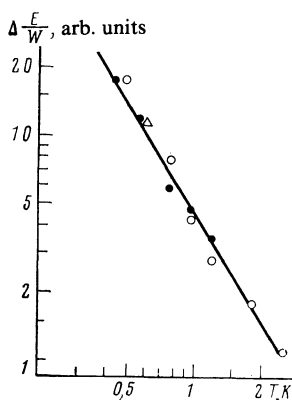


FIG. 6.  $T^2$  dependence of  $\alpha/T$  for samples with the following values of  $\theta$ :  $\bullet$ — $10^\circ 30'$ ;  $\circ$ — $9^\circ 27'$ .

$$\alpha_e = \frac{\pi^2 k^2 T}{3e\varepsilon_F} \left. \frac{\partial \ln \sigma(\varepsilon)}{\partial \ln \varepsilon} \right|_{\varepsilon=\varepsilon_F}, \quad (2)$$

$$\sigma(\varepsilon) = \frac{e^2}{(2\pi)^2} \int \frac{dS_{\mathbf{k}}(\varepsilon)}{\hbar v_{\mathbf{k}}} \mathbf{v}_{\mathbf{k}} \mathbf{l}_{\mathbf{k}},$$

where  $\sigma$  is the conductivity,  $\varepsilon_F$  is the Fermi energy,  $\mathbf{v}_{\mathbf{k}}$  and  $\mathbf{k}$  are the velocity and wave vector of the electrons, the integration is carried out over the Fermi surface, and  $\mathbf{l}_{\mathbf{k}}$  is the vector mean free path, the solution of the kinetic equation

$$\mathbf{v}_{\mathbf{k}} = \int W_{\mathbf{k}\mathbf{k}'} (\mathbf{l}_{\mathbf{k}} - \mathbf{l}_{\mathbf{k}'}) \frac{dS_{\mathbf{k}'}}{\hbar v_{\mathbf{k}'}} \quad (3)$$

where  $W_{\mathbf{k}\mathbf{k}'}$  is the probability for the scattering of electrons by impurities.

Let us assume that the topology of the Fermi surface changes at the point  $\mathbf{k} = 0$ , which is a center of symmetry (cf. Fig. 1). The equation of the Fermi surface near the singularity is

$$\frac{\hbar^2 k_x^2}{2m_x} + \frac{\hbar^2 k_y^2}{2m_y} = \varepsilon_F - \varepsilon_c = \Delta\varepsilon, \quad (4)$$

where  $m_x, m_y > 0$  in the case of the onset of a cavity or  $m_x < 0, m_y > 0$  for the appearance of a neck. For  $\Delta\varepsilon = 0$ , the Fermi velocity  $v_{\mathbf{k}}$  vanishes at the point  $\mathbf{k} = 0$ , giving rise to singularities in the physical properties.<sup>2</sup> For example, for the state density in the 2D case we have

$$v(\varepsilon_F) \sim \int \frac{dS_{\mathbf{k}}}{v_{\mathbf{k}}} = v_{\text{reg}}(\varepsilon_F) + v_{\text{sing}}(\varepsilon_F),$$

$$\frac{v_{\text{sing}}}{v_{\text{reg}}} \sim \begin{cases} \frac{(|m_x| |m_y|)^{1/2}}{m} \ln \left| \frac{\varepsilon_c}{\Delta\varepsilon} \right| & \text{(neck)} \\ \frac{(m_x m_y)^{1/2}}{m} \Theta(\Delta\varepsilon) & \text{(cavity)} \end{cases} \quad (5)$$

where  $m$  is the effective mass characteristic of the large parts of the Fermi surface.

The structural features in the conductivity  $\sigma$  and in the diffuse thermopower  $\alpha_e$  are associated with singularities in  $\mathbf{l}_{\mathbf{k}}$ , which can easily be found from Eq. (3) (Ref. 13). The transition probability  $W_{\mathbf{k}\mathbf{k}'}$ , treated as a function of  $\varepsilon_{\mathbf{k}}$  and  $\varepsilon_{\mathbf{k}'}$ , varies over energy intervals characteristic of the energy spectrum, e.g., the band width, the height of the pseudopotential, etc. In the one-electron approximation, this probability does not depend on the electron population, so it may be assumed regular at  $\Delta\varepsilon = 0$ . The term with  $\mathbf{l}_{\mathbf{k}}$  in (3) has the same singularity as that in the state density (5). In the case in which a neck appears, this term diverges logarithmically as  $\Delta\varepsilon \rightarrow 0$ , while the term with  $\mathbf{l}_{\mathbf{k}'}$  remains finite (because of the condition  $\mathbf{l}_{\mathbf{k}} = 0$  at  $\mathbf{k} = 0$ , a consequence of the odd parity of  $\mathbf{l}_{\mathbf{k}}$ ). We can thus find an explicit expression for  $\mathbf{l}_{\mathbf{k}}$ :

$$\mathbf{l}_{\mathbf{k}} = \frac{\mathbf{v}_{\mathbf{k}}}{\int W_{\mathbf{k}\mathbf{k}'} dS_{\mathbf{k}'} / \hbar v_{\mathbf{k}'}} \equiv \tau_{\mathbf{k}} \mathbf{v}_{\mathbf{k}}, \quad \tau_{\mathbf{k}} \sim \frac{1}{\ln |\varepsilon_c / \Delta\varepsilon|}. \quad (6)$$

In other words, the  $\tau$  approximation turns out to be rigorous (this result is a specific result for the 2D case). In the case in which a cavity appears, we can determine only the nature of the singularity in  $\mathbf{l}_{\mathbf{k}}$ :

$$\mathbf{l}_{\mathbf{k}} = \mathbf{l}_{\mathbf{k}}^{\text{reg}} + \Delta \mathbf{l}_{\mathbf{k}} \Theta(\Delta\varepsilon). \quad (7)$$

Substituting (6) and (7) into (2), we see that  $\sigma^{-1}$  has the same singularities as in the state density (5), and for the singular part of the thermopower  $\alpha_e$  we find (estimating the coefficients in the  $\tau$  approximation)

$$\frac{\alpha_e^{\text{sing}}}{\alpha_e^{\text{reg}}} \sim \begin{cases} \frac{(|m_x| |m_y|)^{1/2}}{m} \frac{v^{\text{reg}}}{v} \frac{\varepsilon_c}{\Delta\varepsilon} & \text{(neck)} \\ -\frac{(m_x m_y)^{1/2}}{m} \delta \left( \frac{\Delta\varepsilon}{\varepsilon_c} \right) & \text{(cavity)} \end{cases} \quad (8)$$

2. *Singularities in  $\alpha_{ph}$ .* To analyze  $\alpha_{ph}$  it is convenient to use the theory of the acoustoelectric effect derived in Ref. 14. In the 2D system a sound wave with wave vector  $\mathbf{q}$ , polarization  $\lambda$ , and energy flux density  $W_{q\lambda}$  excites an electric current

$$\mathbf{j}_{q\lambda}^A = \frac{2\pi e q^2}{(2\pi\hbar)^2 s \omega_{q\lambda} \rho_{2D}} W_{q\lambda} \int dS_{\mathbf{k}} \frac{\Lambda_{\mathbf{k}}^2}{v_{\mathbf{k}}^2} \frac{\partial \mathbf{l}_{\mathbf{k}}}{\partial k_q} \delta(\hat{\mathbf{v}}_{\mathbf{k}} \hat{\mathbf{q}}), \quad (9)$$

where  $\mathbf{l}_{\mathbf{k}}$  is the solution of (3),  $\omega$  and  $s$  are the frequency and velocity of the sound,  $\hat{\mathbf{v}}_{\mathbf{k}}$  and  $\hat{\mathbf{q}}$  are unit vectors along the directions of  $\mathbf{v}_{\mathbf{k}}$  and  $\mathbf{q}$ ,  $\Lambda_{\mathbf{k}}$  is the corresponding component of the strain potential,  $k_q = \mathbf{k} \hat{\mathbf{q}}$ , and  $\rho_{2D}$  is the density of the metal. Under the experimental conditions the phonons are scattered primarily at the boundaries of the sample, so that the phonon energy flux  $W_{q\lambda}$  produced by the temperature gradient can be assumed given, independent of the properties of the electron system. To derive the thermoelectric current we need to sum<sup>3)</sup> expression (9) over  $\mathbf{q}$  and  $\lambda$ . We then find an expression

$$\alpha_{ph}^{ij} = \sigma_{ij}^{-1} \sum_{\lambda} \int d\Omega_{\hat{\mathbf{q}}} \int dS_{\mathbf{k}} \frac{F^i(\hat{\mathbf{q}}, \lambda)}{v_{\mathbf{k}}^2} \left( \frac{\partial l_{\mathbf{k}}^j}{\partial k} \hat{\mathbf{q}} \right) \delta(\hat{\mathbf{v}}_{\mathbf{k}} \hat{\mathbf{q}}) \quad (10)$$

for the thermopower, where the function  $F(\hat{\mathbf{q}})$  has the property  $F(\hat{\mathbf{q}}) = -F(-\hat{\mathbf{q}})$ . In the  $\tau$  approximation for phonons this function is

$$F(\mathbf{q}, \lambda) = \frac{\pi}{30} T^3 \frac{e \Lambda^2 l_{ph}}{(\hbar s)^5 \rho_{2D}} v_{q\lambda}, \quad (11)$$

where  $l_{ph}$  is the phonon mean free path.

An integration over the directions of  $\mathbf{q}$  in (10) eliminates the  $\delta$ -function. Assuming that the symmetry plane passes through  $\mathbf{k} = 0$ , we find

$$\alpha_{ph}^{xx} = \frac{2}{\sigma^{xx}} \sum_{\lambda} \int dS_{\mathbf{k}} \frac{F^x(\hat{\mathbf{t}}_{\mathbf{k}}, \lambda)}{v_{\mathbf{k}}^2} \frac{\partial l^x}{\partial k_x} \hat{\mathbf{t}}_{\mathbf{k}}^x, \quad (12)$$

where  $\hat{\mathbf{t}}_{\mathbf{k}}$  is the vector tangent to the Fermi surface at the point  $\mathbf{k}$ , and we find an analogous expression for  $\alpha_{ph}^{yy}$ . When a neck appears, we have, by virtue of (6) and (4),

$$\left. \frac{\partial l^x}{\partial k_x} \right|_{\mathbf{k}=0} = \frac{\hbar \tau}{m_x} < 0, \quad \left. \frac{\partial l^y}{\partial k_y} \right|_{\mathbf{k}=0} = \frac{\hbar \tau}{m_y} > 0. \quad (13)$$

We see from these results that the singularities in  $\alpha_{ph}^{xx}$  and  $\alpha_{ph}^{yy}$  (i.e., in measurements along and across the neck) are of opposite sign.

Because of the square of  $V_{\mathbf{k}}$  in the denominator of the integrand in (12), the singularities in  $\alpha_{ph}$  turn out to be stronger than those in the state density:

$$\frac{\alpha_{ph}^{xx \text{ sing}}}{\alpha_{ph}^{xx \text{ reg}}} \sim \begin{cases} -A \frac{v}{v_{\text{reg}}} \left( \frac{\varepsilon_c}{|\Delta\varepsilon|} \right)^{1/2} & \text{(neck)} \\ B \frac{v}{v_{\text{reg}}} \left( \frac{\varepsilon_c}{\Delta\varepsilon} \right)^{1/2} \Theta(\Delta\varepsilon) & \text{(cavity)} \end{cases} \quad (14)$$

where

$$A = \frac{m_y}{[m(|m_x| + |m_y|)]^{1/2}} E \left( \left[ \frac{|m_y|}{|m_x| + |m_y|} \right]^{1/2} \right),$$

$$m_y \Delta\varepsilon > 0,$$

$$A = \frac{m_y}{[m(|m_x| + |m_y|)]^{1/2}} \left\{ K \left( \left[ \frac{|m_x|}{|m_x| + |m_y|} \right]^{1/2} \right) - E \left( \left[ \frac{|m_x|}{|m_x| + |m_y|} \right]^{1/2} \right) \right\}, \quad m_y \Delta\varepsilon < 0,$$

$$B = \frac{m_x}{m_y - m_x} \left( \frac{m_y}{m} \right)^{1/2} \left\{ \frac{m_y}{m_x} E \left( \left[ \frac{m_y - m_x}{m_y} \right]^{1/2} \right) - K \left( \left[ \frac{m_y - m_x}{m_y} \right]^{1/2} \right) \right\}, \quad m_y \geq m_x,$$

$$B = -\frac{m_y}{m_x - m_y} \left( \frac{m_x}{m} \right)^{1/2} \left\{ K \left( \left[ \frac{m_x - m_y}{m_x} \right]^{1/2} \right) - E \left( \left[ \frac{m_x - m_y}{m_x} \right]^{1/2} \right) \right\}, \quad m_y \leq m_x.$$

The coefficients have been estimated for  $W_{kk'} = \text{const}$ ,  $A = \text{const}$ , and  $l_{ph} = \text{const}$ ;  $E(k)$  and  $K(k)$  are elliptic integrals. Expressions for  $\alpha_{ph}^{yy}$  can be found from (14) by interchanging  $x$  and  $y$ .

The logarithmic singularity in  $\mathbf{l}_k$  in (6) cancels out with a similar singularity in  $\sigma$ , so that no singularities of kinetic origin are found in  $\alpha_{ph}$  in the case in which a neck appears. In the case in which a cavity sets in, the singularity in  $\mathbf{l}_k$  in (7) cancels out with one in  $\sigma$  only under conditions such that the  $\tau$  approximation is applicable (e.g., with  $W_{kk'} = \text{const}$ ); in general, this singularity gives rise to an additional jump in  $\alpha_{ph}$  (Fig. 7), given by

$$\tilde{\alpha}_{ph}^{\text{sing}} = \text{const} \Theta(\Delta\varepsilon). \quad (15)$$

**3. Factors limiting the singularities.** In the discussion above we assumed

$$\frac{T}{\varepsilon_F} \rightarrow 0, \quad \frac{\hbar}{\varepsilon_F \tau} \rightarrow 0, \quad \frac{q_T}{k_F} \rightarrow 0, \quad (16)$$

$$\frac{1}{q_T l_F} \rightarrow 0, \quad \frac{s}{v_F} \rightarrow 0,$$

where  $\tau$  is the electron relaxation time,  $l_F = \tau v_F$  is the electron mean free path, and  $q_T = T/\hbar s$  is the thermal momentum of the phonons. A nonzero value of any of the parameters in (16) may lead to a cutoff of the singularities. The effect of the first parameter is associated with a spreading of the Fermi distribution; while that of the second is associated with the impurity spreading of the spectrum. These two parameters cut off the singularities in both  $\alpha_e$  and  $\alpha_{ph}$ .

The three other parameters in (16) are important only for  $\alpha_{ph}$ , and they lead to a shrinkage, rather than elimination, of the singularities, as we will see.

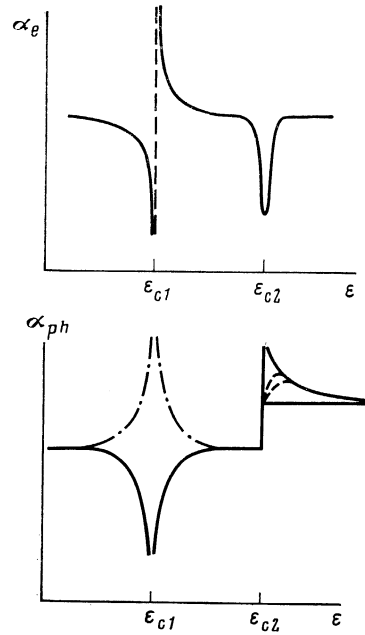


FIG. 7. Calculated changes in the diffuse and phonon components,  $\alpha_e$  and  $\alpha_{ph}$ , respectively, of the thermopower in the 2D electron system at the topological transitions.  $C_1$ —Appearance of a neck;  $C_2$ —onset of a cavity.

To study the role of the parameter  $q_T/k_F$  we note that the  $\delta$ -function in (9) and (10) arises from the  $\delta$ -function which expresses energy conservation,

$$\delta(\varepsilon_{\mathbf{k}+\mathbf{q}} - \varepsilon_{\mathbf{k}} - \hbar\omega_{\mathbf{q}}) \approx \delta(\hbar\mathbf{v}_{\mathbf{k}}\mathbf{q} - \hbar\omega_{\mathbf{q}} + \frac{\hbar^2 q_x^2}{2m_x} + \frac{\hbar^2 q_y^2}{2m_y} + \dots) \rightarrow \frac{\delta(\hat{\mathbf{v}}_{\mathbf{k}}\hat{\mathbf{q}})}{v_{\mathbf{k}}q}, \quad (17)$$

as a result of an expansion of the argument in  $\mathbf{q}$  and the retention of only the first term. This simplification is justified if  $\Delta\varepsilon \gg \hbar^2 q_T^2/m$ , since in this case the minimum value of  $v_{\mathbf{k}}$  on the Fermi surface is large in comparison with  $\hbar q_T/m$ , and the first term in (17) is the leading term. In a small neighborhood of the transition  $\Delta\varepsilon \ll \hbar^2 q_T^2/m$ , we can ignore the term  $\hbar\mathbf{v}_{\mathbf{k}}\mathbf{q}$  near the point  $\mathbf{k} = 0$  in (17) in comparison with the terms  $q^2$ . In the case in which a neck appears ( $m_x < 0$ ,  $m_y > 0$ ), this simplification does not interfere with the vanishing of the argument of the  $\delta$ -function in the integration over the directions of  $\mathbf{q}$ . Here the power of  $v_{\mathbf{k}}$  in the denominator in (12) decreases from the second to the first, and the singularity in  $\alpha_{ph}$  shrinks:

$$\alpha_{ph}^{\text{sing}} \sim \infty \ln|\varepsilon_c/\Delta\varepsilon|, \quad \Delta\varepsilon/\varepsilon_c \ll (q_T/k_F)^2 \quad \text{(neck)}.$$

When a cavity appears ( $m_x > 0$ ,  $m_y > 0$ ), the argument of the  $\delta$ -function does not vanish at  $\Delta\varepsilon \lesssim \hbar^2 q_T^2/m$ , and the singularity at  $\Delta\varepsilon = 0$  is eliminated. This effect results from the physically obvious circumstance that a cavity of size  $k_0 \lesssim q_T$  does not interact with phonons. The Kohn singularity which arises at  $k_0 \sim q_T$  smoothes out to become a regular maximum after an integration over the phonon thermal distribution (Fig. 7). The singularity of kinetic origin, (15) persists.

To study the role played by the parameter  $q_T l$ , we follow Pippard,<sup>16</sup> replacing the  $\delta$ -function in (10) by a Lorentzian function:

$$\delta(\hat{\mathbf{v}}_{\mathbf{k}}\hat{\mathbf{q}}) = \delta(\cos\varphi) \rightarrow \frac{1}{\pi} \frac{q_{\parallel}\mathbf{k}}{1+(q_{\parallel}\mathbf{k})^2 \cos^2\varphi} = \frac{1}{\pi} \frac{q_{\parallel}v_{\mathbf{k}}}{1+(q_{\parallel}v_{\mathbf{k}})^2}. \quad (18)$$

Near  $\mathbf{k} = 0$ , the velocity vanishes,  $v_{\mathbf{k}} \rightarrow 0$ , and we can discard the term  $(q_{\parallel}v_{\mathbf{k}})^2$  in the denominator in (18). As a result, the power of  $V_{\mathbf{k}}$  in the denominator in (10) decreases by one, and the singularity in  $\alpha_{ph}$  weakens to the size of the singularities in the state density, (5). This is true only if  $\Delta\varepsilon \lesssim \varepsilon_c/(q_T l_F)^2$ , since in the opposite case the minimum value of  $v_{\mathbf{k}}$  on the Fermi surface would be greater than  $1/q_T \tau$ , and it would be legitimate to use a  $\delta$ -function in place of (18).

To study the effects  $\sim s/v_F$  in the  $\delta$ -function in (17), we need to retain the term  $\hbar\omega_q$ . The condition for the vanishing of its argument,

$$v_{\mathbf{k}}\hat{\mathbf{q}} = s, \quad (19)$$

can hold only on those parts of the Fermi surface for which the condition  $v_{\mathbf{k}} \geq s$  holds. As a result, the singularities at  $\varepsilon = \varepsilon_c$ , associated with the vanishing of  $v_{\mathbf{k}}$ , are eliminated [only the "kinetic" singularities, (15), remain]. In their place we find singularities at the point  $\varepsilon = \varepsilon_{c1}$ , where the parts of the Fermi surface which do not interact with phonons ( $v_{\mathbf{k}} < s$ ) first appear, and at the point  $\varepsilon = \varepsilon_{c2}$ , where these regions disappear.

Substituting the  $\delta$ -function in (17) into (10), retaining the term  $\hbar\omega_q$ , and integrating, we find

$$\alpha_{ph}^{\infty} = \frac{1}{\Omega_{xx}} \sum_{\alpha=1,2} \sum_{\lambda} \int dS_{\mathbf{k}} \frac{F^{\lambda}(\hat{\mathbf{q}}_{\mathbf{k}}^{\alpha}, \lambda)}{v_{\mathbf{k}}(v_{\mathbf{k}}^2 - s^2)^{1/2}} \frac{\partial I_{\mathbf{k}}^{\lambda}}{\partial k_x} (\hat{\mathbf{q}}_{\mathbf{k}}^{\alpha})^{\alpha} \Theta(v_{\mathbf{k}} - s), \quad (20)$$

where  $\hat{\mathbf{q}}_{\mathbf{k}}^{\alpha}$  ( $\alpha = 1, 2$ ) are the solutions of (19). In general, the singularity in the integrand at  $v_{\mathbf{k}} = s$  is integrable and does not result in singularities in  $\alpha_{ph}$ . An exceptional case is that in which the velocity  $v_{\mathbf{k}}$  has an extremum on the Fermi surface, at which its value is  $s$ :

$$v_{ext} = s. \quad (21)$$

This condition can hold only at isolated points on the  $\varepsilon$  axis; for spectrum (4), these points are

$$\varepsilon_{c1} = \varepsilon_c + m_x s^2/2, \quad \varepsilon_{c2} = \varepsilon_c + m_y s^2/2. \quad (22)$$

It should be kept in mind that for the extrema in (21) the vectors  $\hat{\mathbf{q}}_{\mathbf{k}}$ , which are the solutions of (19), are generally oriented along a direction of a high crystallographic symmetry, and the function  $F^{\lambda}(\hat{\mathbf{q}})$  in (20) may vanish. For spectrum (4), the vectors  $\hat{\mathbf{q}}_{\mathbf{k}}$  at the extrema are directed along the  $x$  axis at  $\varepsilon = \varepsilon_{c1}$  and along the  $y$  axis at  $\varepsilon = \varepsilon_{c2}$ . Making use of the behavior of  $F^{\lambda}(\hat{\mathbf{q}})$  near  $\hat{\mathbf{q}} = \hat{\mathbf{x}}$  and  $\hat{\mathbf{q}} = \hat{\mathbf{y}}$   $F^x(\hat{\mathbf{q}}) \sim \text{const}$ ,  $F^y(\hat{\mathbf{q}}) \sim q_y$ ,  $q_y \rightarrow 0$ ;  $F^x(\hat{\mathbf{q}}) \sim q_x$ ,  $F^y(\hat{\mathbf{q}}) \sim \text{const}$ ,  $q_x \rightarrow 0$ , we find the following expressions for  $\alpha_{ph}$  near the singularities:

$$\alpha_{ph}^{\infty} \sim \ln \frac{1}{|\varepsilon_F - \varepsilon_{c1}|}, \quad \alpha_{ph}^{yy} \sim (\varepsilon_F - \varepsilon_{c1}) \ln \frac{1}{|\varepsilon_F - \varepsilon_{c1}|}, \quad \varepsilon_F \rightarrow \varepsilon_{c1} \quad (23)$$

$$\alpha_{ph}^{\infty} \sim (\varepsilon_F - \varepsilon_{c2}) \ln \frac{1}{|\varepsilon_F - \varepsilon_{c2}|}, \quad \alpha_{ph}^{xx} \sim \ln \frac{1}{|\varepsilon_F - \varepsilon_{c2}|}, \quad \varepsilon_F \rightarrow \varepsilon_{c2}.$$

The singularities are of the same type for the cases in which a cavity and a neck appear, but in the former case the two

singularities lie in the same side of the point  $\varepsilon = \varepsilon_c$ , and in the latter case they lie on different sides [see (22)].

Consequently, the finite size of the parameter  $s/v_F$  gives rise to a splitting of the singularities in the region  $\Delta\varepsilon \sim ms^2 \sim \varepsilon_c (s/v_F)^2$ . For superlattices on silicon with a period  $d \sim 10a$ , we have  $s/v_F \approx 1/30$ , and the splitting is too small. This splitting would apparently be observable for superlattices with a period several times greater.

**4. Role of the 3D nature of the phonons.** Up to this point we have been dealing with an idealized model of the 2D system. We will now discuss the extent to which this idealization is applicable for describing the processes in real metal-insulator-semiconductor structures. That the electron gas in these systems is a 2D system is beyond doubt: The electrons are localized in a thin layer of thickness  $d \sim 50 \text{ \AA}$  near the surface of the semiconductor, in a lower quantum-size level. Their wave functions can be written

$$\psi_{\mathbf{k}_{\parallel}} = S^{-1/2} \exp(i\mathbf{k}_{\parallel}\mathbf{r}_{\parallel}) \Phi(z), \quad (24)$$

where  $\mathbf{k}_{\parallel} = (k_x, k_y)$ ,  $\mathbf{r}_{\parallel} = (x, y)$ ,  $S$  is the area of the surface, and  $\Phi(z)$  is a normalized function, nonzero in the region  $0 \leq z \leq d$ . The phonons in metal-insulator-semiconductor structures, in contrast, are a 3D system, free to move over the entire thickness of the sample, as is verified by estimates of the thermal conductivity and of the phonon-drag thermopower  $\alpha_{ph}$  (Ref. 17). The 3D nature of the phonons should be taken into account in a discussion of the singularities in  $\alpha_{ph}$ .

The probability for the electron-phonon interaction is known<sup>10</sup> to contain the square of the matrix element of the phonon wave between electron wave functions:

$$J = \left| \int d\mathbf{r} \psi_{\mathbf{k}'}^*(\mathbf{r}) e^{i\mathbf{q}\cdot\mathbf{r}} \psi_{\mathbf{k}}(\mathbf{r}) \right|^2. \quad (25)$$

In the 3D case,  $\psi_{\mathbf{k}}$  is a 3D plane wave, and  $J$  reduces to  $\delta_{\mathbf{k}' - \mathbf{k} - \mathbf{q}}$ . For wave functions as in (24) we find

$$J = \delta_{\mathbf{k}_{\parallel}' - \mathbf{k}_{\parallel} - \mathbf{q}_{\parallel}} I(q_z),$$

where  $I(q_z)$  can be evaluated easily in two limiting cases,

$$I(q_z) = \left| \int dz \Phi^*(z) e^{iq_z z} \Phi(z) \right|^2 = \begin{cases} 1, & qd \ll 1 \\ d^{-1} \delta(q_z), & qd \gg 1 \end{cases} \quad (26)$$

[in the former case we can set  $e^{iq_z z} = 1$ ; in the second case, the integral is significantly different from zero at  $q_z d \lesssim 1$ , and the quantity  $I(q_z)d$  has the properties of a  $\delta$ -function]. Making this modification of the probability for the electron-phonon interaction, we calculate the acoustoelectric current:

$$\mathbf{j}^A = \frac{2\pi e q^2}{(2\pi\hbar)^2 \rho_{3D} s \omega_{\mathbf{q}}} W_{\mathbf{q}\lambda} I(q_z) \times \int dS_{\mathbf{k}} \frac{\Lambda_{\mathbf{k}}^2}{v_{\mathbf{k}}^2} \frac{\partial I_{\mathbf{k}}}{\partial k_{q_{\parallel}}} \delta\left(\hat{v}_{\mathbf{k}} \frac{q}{q_{\parallel}} - s \frac{q}{q_{\parallel}}\right) \quad (27)$$

[ $\mathbf{k} = (k_x, k_y)$  is a 2D vector]. To calculate the thermal electric current we need to integrate over the 3D phonon momentum  $\mathbf{q}$ . If  $q_T d \gg 1$ , we find, after a trivial integration over  $q_z$ , expression (10) for  $\alpha_{ph}$  with  $q_{\parallel}$  instead of  $q$  and with a correspondingly defined function  $F(\hat{\mathbf{q}})$ . In the case  $q_T d \lesssim 1$ , expression (27) reduces to the form of (10) if we ignore effects

$\sim s/v_F$ . Let us write the functions  $F(\mathbf{q})$  in the  $\tau$  approximation for the phonons:

$$F(\hat{\mathbf{q}}) = \frac{\pi}{30} T^3 \frac{e\Lambda^2 l_{ph}}{(\hbar s)^5 \rho_{3D}} \frac{1}{2\pi d} \hat{s}\mathbf{q}, \quad q_T d \gg 1,$$

$$F(\hat{\mathbf{q}}) = \frac{5! \zeta(5)}{32\pi^3} T^4 \frac{e\Lambda^2 l_{ph}}{(\hbar s)^6 \rho_{3D}} \hat{s}\mathbf{q}, \quad q_T d \ll 1. \quad (28)$$

Consequently, all the results of Subsec. 2 and 3 apply to metal-insulator-semiconductor structures in the case  $q_T d \gg 1$ , and all the results except (23) apply in the case  $q_T d \lesssim 1$ . In this latter case, (23) are replaced by

$$\alpha_{ph}^{xx\infty} (\varepsilon_{c1} - \varepsilon_F)^{1/2} \Theta(\varepsilon_{c1} - \varepsilon_F),$$

$$\alpha_{ph}^{yy\infty} (\varepsilon_{c1} - \varepsilon_F)^{3/2} \Theta(\varepsilon_{c1} - \varepsilon_F), \quad \varepsilon_F \rightarrow \varepsilon_{c1}, \quad (29)$$

$$\alpha_{ph}^{xx\infty} (\varepsilon_{c2} - \varepsilon_F)^{3/2} \Theta(\varepsilon_{c2} - \varepsilon_F),$$

$$\alpha_{ph}^{yy\infty} (\varepsilon_{c2} - \varepsilon_F)^{1/2} \Theta(\varepsilon_{c2} - \varepsilon_F), \quad \varepsilon_F \rightarrow \varepsilon_{c2}.$$

To derive these expressions we integrate over  $d^3 q$  in (27) in polar coordinates. After an integration over  $q$  and  $\varphi$ , the integrand has a singularity of the type in (23), but with the sound velocity

$$\tilde{s} = s / \sin \theta$$

instead of  $s$  [see (22)]. Replacing  $s$  by  $\tilde{s}$  in (23), and integrating over  $\theta$ , we find (29).

Finally, we write expressions for  $\alpha_{ph}$  for a spherical Fermi surface (far from a topological transition):

$$\alpha_{ph} = \frac{\pi}{30} \frac{k}{e} (kT)^3 \frac{m^2}{N_S \hbar k_F} \frac{s}{(\hbar s)^5 d \rho_{3D}} \Lambda^2 l_{ph}, \quad q_T d \gg 1, \quad (30a)$$

$$\alpha_{ph} = \frac{5! \zeta(5)}{16\pi^2} \frac{k}{e} (kT)^4 \frac{m^2}{N_S \hbar k_F} \frac{s}{(\hbar s)^6 \rho_{3D}} \Lambda^2 l_{ph}, \quad q_T d \ll 1. \quad (30b)$$

Expression (30a) gives a satisfactory description of measurements of  $\alpha_{ph}$  in metal-insulator-semiconductor structures<sup>12</sup> and in conducting layers on germanium surfaces<sup>4</sup> (Ref. 17).

#### 4. DISCUSSION OF RESULTS

Working from the known energy spectrum of the 2D electrons in the samples with a superlattice (Fig. 1), we would expect to find two topological transitions in the range of densities  $N_S$  studied. We identify these two transitions with points  $A$  and  $B$  (Fig. 2); the first is associated with the appearance of a neck, and the second with the onset of a new cavity.

Comparison of the experimental data (Fig. 2) with theoretical results (Fig. 7) shows that the structural features observed in  $\alpha$  in the region of the topological structure are associated with changes in both  $\alpha_e$  and  $\alpha_{ph}$  and are a superposition of curves  $a$  and  $b$  in Fig. 7. For example, feature  $A$  consists of a maximum and minimum separated by a sharp jump, as in the theoretical structural feature,  $\alpha_e^{\text{sing}} \propto (\Delta\varepsilon)^{-1}$ . For  $\alpha^{xx}$ , however (for the case in which the heat flux is directed along the neck), the minimum is significantly deeper than the maximum is high, while for  $\alpha^{yy}$  the maximum is larger than the minimum. This fact can be explained in a natural way as due to  $\alpha_{ph}$ , which is predicted theoretically to

be negative in the former case ( $\alpha_{xx}^{\text{sing}} \propto -|\Delta\varepsilon|^{-1/2}$ ) and positive in the latter ( $\alpha_{yy}^{\text{sing}} \propto -|\Delta\varepsilon|^{-1/2}$ ).

For structural feature  $B$  the minimum should be interpreted as an  $\alpha_e$  contribution of the type ( $\alpha_e^{\text{sing}} \propto -\delta(\Delta\varepsilon)$ ), and the maximum as an  $\alpha_{ph}$  contribution of the type ( $\alpha_{ph}^{\text{sing}} \propto (\Delta\varepsilon)^{-1/2} \Theta(\Delta\varepsilon)$ ). As the centers of the structural features (the arrows in Fig. 2) we choose the position of the minimum of the curve for  $\alpha_{xx}$  for feature  $A$  and the position of the maximum for  $\alpha_{yy}$ ; for feature  $B$  we choose the position of the minimum of  $\alpha$ . These characteristic points undergo the least shift upon a change in temperature.

The clear manifestation of both  $\alpha_e^{\text{sing}}$  and  $\alpha_{ph}^{\text{sing}}$  on the experimental curves is evidence for a relation  $\alpha_e^{\text{sing}} \sim \alpha_{ph}^{\text{sing}}$ . At the same time, the data in Fig. 5 show that at the lowest temperatures ( $T \sim 0.5 K$ ) we have  $\alpha_e^{\text{reg}} \sim 5\alpha_{ph}^{\text{reg}}$ , so that the relative size of the structural feature,  $\alpha_{ph}^{\text{sing}}/\alpha_{ph}^{\text{reg}}$ , should be much greater than  $\alpha_e^{\text{sing}}/\alpha_e^{\text{reg}} \sim 1$ .

To estimate the size of the structural features, we write numerical values for the cutoff factors which we used above:

$$\frac{T}{\varepsilon_F} \approx \frac{1}{400} - \frac{1}{200}, \quad \frac{\hbar}{\varepsilon_F \tau} \approx \frac{1}{30} - \frac{1}{40}, \quad \frac{q_T}{k_F} \approx \frac{1}{3} - \frac{1}{6},$$

$$q_T l \approx \frac{1}{10} - \frac{1}{30}, \quad \frac{s}{v_F} \approx \frac{1}{30}$$

( $\varepsilon_F$  and  $k_F$  are calculated from  $N_A$ , while the time  $\tau$  is calculated from the mobility  $\mu$ ). We see that the primary cutoff factor for  $\alpha_e$  is  $\hbar/\varepsilon_F \tau$ , while that for  $\alpha_{ph}$  is the ratio  $q_T/k_F$ . Using these values, we find the following estimate of the size of the structural features at the minimum of  $A$ :

$$\frac{\alpha_e^{\text{sing}}}{\alpha_e^{\text{reg}}} \sim \frac{(|m_x| m_y)^{1/2}}{m} \frac{\varepsilon_F \tau}{\hbar} \sim 10, \quad \frac{\alpha_{ph}^{\text{sing}}}{\alpha_{ph}^{\text{reg}}} \sim \frac{k_F}{q_T} \sim 3-6.$$

In the former case, the size of the structural feature predicted by the calculation is an order of magnitude greater than the experimental values. A possible explanation for the discrepancy is that the estimates in (8) and (14) were derived in the  $\tau$  approximation. Estimates (31) can be reconciled with the experimental results by assuming that the value of  $\tau$  near the singularity  $\mathbf{k} = 0$  is much smaller than the average value over the Fermi surface.

The temperature dependence of the absolute size of the structural features is determined by the changes in the cutoff factors. As we mentioned earlier, the quantity  $\alpha_e^{\text{sing}}/\alpha_e^{\text{reg}}$  is determined by  $\hbar/\varepsilon_F \tau$  and is thus independent of the temperature, while  $\alpha_{ph}^{\text{sing}}/\alpha_{ph}^{\text{reg}}$  is determined by  $q_T/k_F$  and should increase in inverse proportion to the temperature. The quantity  $E/W$ , used in analyzing the experimental data, is proportional to  $a/T^2 + b$  according to (1). Consequently, depending on whether the structural feature in  $\alpha$  comes primarily from  $\alpha_e$  or  $\alpha_{ph}$ , we conclude that  $\Delta(E/W)$  will vary either as  $T^{-2}$  or as  $T^{-1}$ . This conclusion is not in contradiction of the experimental results (Fig. 5), which yield  $\Delta(E/W) \sim T^{-1.6}$ .

We are primarily interested in determining the behavior of the thermopower near the structural features and in relating this behavior to the theory. The change in the surface density  $N_S$  of the 2D electron gas is related to the change in the Fermi level  $\varepsilon_F$  by the obvious relation

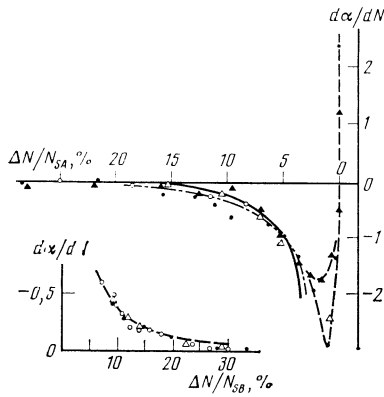


FIG. 8. Behavior of the height of the singularity near the topological transition. Solid line—Behavior proportional to  $(\Delta N_S)^{-2}$ ; dot-dashed line— $(\Delta N_S)^{-1.5}$ ; dashed curves—change in the region of the thermal spreading [●—0.45 K; ▲—0.58 K].  $\theta$ :  $\triangle$ — $9^\circ$ ;  $\circ$ — $9^\circ 27'$ ; ●, ▲— $10^\circ 30'$ .

$$\Delta N_S = v(\epsilon_F) \Delta \epsilon_F.$$

The state density  $v(\epsilon_F)$  has weak structural features (5) at the points of the topological transitions. Because of the spreading, these structural features are nearly indistinguishable (as is clear from the conductivity measurements), and near the transition  $N_S$  and  $\epsilon_F$  may be assumed proportional. For  $\alpha_{xx}$  we consider the left wing of peak  $A$  and the right wing of  $B$ . (In the gap, the features  $A$  and  $B$  distort each other greatly.) To eliminate the regular part of  $\alpha$ , we consider the derivative of  $\alpha$  with respect to  $\epsilon$ , which is proportional to  $d\alpha/dN_S$ . To calculate  $d\alpha/dN_S$ , we use the experimental points (Fig. 8). For the sample with  $\theta = 9^\circ$ , the curve of  $d\alpha/dN_S$  is displaced  $-0.6$  along the ordinate axis, so that we have  $d\alpha/dN_S \rightarrow 0$  with  $\Delta N_S/N_A \approx 20\%$ . Outside the region of the temperature spreading (the dashed curve) the behavior of  $\alpha$  near the singularity is described by

$$d\alpha/d\epsilon \sim |\epsilon_F - \epsilon_c|^{1.7 \pm 0.3}.$$

This result is consistent with the theoretical conclusions, which show that the exponent should be between  $-1.5$  (the dot-dashed line) and  $-2$  (the solid line in Fig. 8), depending on whether  $\alpha_{ph}$  or  $\alpha_e$  is predominant for feature  $A$ , while the exponent should be  $-1.5$  for feature<sup>5)</sup>  $B$ .

For peak  $B$ , the maximum of  $\alpha$  corresponds to the condition  $q_T \sim k_0$ , where  $k_0$  is the size of the cavity. As the temperature changes, the distance between the maximum of  $\alpha$  and the center of peak  $B$  increases approximately linearly (Fig. 9). This behavior is consistent with the behavior of the size of the cavity if we ignore the pseudopotential splitting,  $k_0 \sim (\epsilon_F - \epsilon_{cB})$ , as we may for sufficiently large cavities.

The positions of the points of the topological transitions,  $A$  and  $B$ , depend on the period of the superlattice in question or on the angle ( $\theta$ ) between the surface on which the metal-insulator-semiconductor structure is fabricated and the (100) Si plane (Fig. 4). If the superlattice pseudopotential is ignored, the two transitions would occur at the same point, whose position could be determined from the tangency of the two Fermi spheres in Fig. 1. Their radius  $k_F$  would correspond to the distance from the center of the electron valleys,  $0.15(2\pi/a)\sin\theta$  (for Si,  $a = 543 \text{ \AA}$ ), to the boundary of the

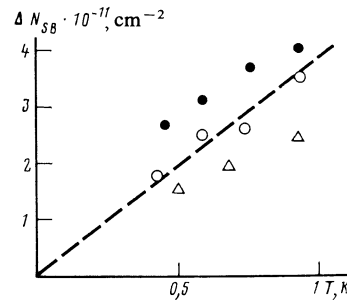


FIG. 9. Temperature dependence of the distance from  $B$  to the maximum of  $\alpha_{||}$  for samples with the following values of  $\theta$ :  $\triangle$ — $9^\circ$ ;  $\circ$ — $9^\circ 27'$ ; ●— $10^\circ 30'$ .

Brillouin zone. The results of an estimate of  $N_A$  found in this manner (the solid curve in Fig. 4) agree reasonably well with experiment. The reason why structural features  $A$  and  $B$  are positioned asymmetrically with respect to the solid line appears to be some distortion ( $\propto \cos\theta$ ) of the shape of the electron valleys.

The distance between peaks  $A$  and  $B$  determines the size of the minigap,  $\Delta$ . A calculation of  $\Delta$  from the experimental values of  $N_B - N_A$  and the average state density,  $v(\epsilon_F) = 1.6 \cdot 10^{11} \text{ cm}^{-2} \cdot \text{meV}^{-1}$ , yields a result in agreement with direct measurements of  $\Delta$  (Refs. 18 and 19).

We thank A. F. Andreev, M. I. Kaganov, and A. I. Shal'nikov for discussions, Z. D. Kvon for participation in the initial part of this study, and N. A. Nikitin for technical cooperation.

<sup>1)</sup>Continuous measurements were impeded by the long times required for relaxation to the equilibrium density  $N_S(V_g)$ .

<sup>2)</sup>The diffuse component of the thermopower is  $\alpha_e^{\text{exp}} = 1.3 \cdot 10^{-6} T \text{ V/C}$ . An estimate for a free electron gas yields  $\alpha_e \sim \pi^2 k^2 T / 3 |e| \epsilon_F = 1.9 \cdot 10^{-6} T \text{ V/C}$ .

<sup>3)</sup>See Ref. 15 for more details on the relationship between the thermopower and the acoustoelectric effect.

<sup>4)</sup>There are some errors in the calculation of  $\alpha_{ph}$  in the Appendix to Ref. 17.

<sup>5)</sup>At extremely low temperatures,  $T \lesssim 0.5 \text{ K}$ , irregularities appear at the left on the  $\alpha(N_S)_A$  curves. These irregularities cause a scatter of the points on the curve in Fig. 8 from the smooth behavior (see, for example, the results for  $\theta = 10^\circ 30'$ ,  $\Delta N \sim 10\% N_A$ ).

<sup>1)</sup>I. M. Lifshitz, Zh. Eksp. Teor. Fiz. **38**, 1569 (1960) [Sov. Phys. JETP **11**, 1130 (1960)].

<sup>2)</sup>M. I. Kaganov and I. M. Lifshitz, Usp. Fiz. Nauk **129**, 487 (1979) [Sov. Phys. Usp. **22**, 904 (1979)].

<sup>3)</sup>N. B. Brandt, N. I. Ginzburg, T. A. Ignat'eva, et al., Zh. Eksp. Teor. Fiz. **49**, 85 (1965) [Sov. Phys. JETP **22**, 61 (1966)].

<sup>4)</sup>D. R. Overcash, T. Davis, J. W. Cook, Jr., and M. J. Skove, Phys. Rev. Lett. **46**, 287 (1981).

<sup>5)</sup>S. L. Bud'ko, A. N. Voronovskii, A. G. Gopotchenko, and E. S. Itskevich, Zh. Eksp. Teor. Fiz. **86**, 778 (1984) [Sov. Phys. JETP **59**, 454 (1984)].

<sup>6)</sup>V. S. Egorov and A. N. Fedorov, Zh. Eksp. Teor. Fiz. **85**, 1647 (1983) [Sov. Phys. JETP **58**, 959 (1983)].

<sup>7)</sup>V. A. Volkov, V. B. Petrov, and V. A. Sandomirskii, Usp. Fiz. Nauk **131**, 423 (1980) [Sov. Phys. Usp. **23**, 375 (1980)].

<sup>8)</sup>T. Cole, A. A. Lakhani, and P. J. Stiles, Phys. Rev. Lett. **38**, 722 (1977).

<sup>9)</sup>N. V. Zavaritskii and Z. D. Kvon, Pis'ma Zh. Eksp. Teor. Fiz. **39**, 61 (1984) [JETP Lett. **39**, 71 (1984)].

<sup>10)</sup>J. M. Ziman, Electrons and Phonons, Oxford Univ. Press, London, 1960 (Russ. transl. IIL, Moscow, 1962).

<sup>11)</sup>N. V. Zavaritskii and A. N. Vetchinkin, Prib. Tekh. Eksp. No. 1, 247 (1974).

- <sup>12</sup>N. V. Zavaritskiĭ and Z. D. Kvon, *Pis'ma Zh. Eksp. Teor. Fiz.* **38**, 85 (1983) [*JETP Lett.* **38**, 97 (1983)].
- <sup>13</sup>V. G. Vaks, A. V. Trefilov, and S. V. Fomichev, *Zh. Eksp. Teor. Fiz.* **80**, 1613 (1981) [*Sov. Phys. JETP* **53**, 830 (1981)].
- <sup>14</sup>M. I. Kaganov, Sh. T. Mevlyut, and I. M. Suslov, *Zh. Eksp. Teor. Fiz.* **78**, 376 (1980) [*Sov. Phys. JETP* **51**, 189 (1980)].
- <sup>15</sup>I. M. Suslov, *Zh. Eksp. Teor. Fiz.* **85**, 1847 (1983) [*Sov. Phys. JETP* **58**, 1074 (1983)].

- <sup>16</sup>A. B. Pippard, *Proc. R. Soc. London* **A257**, 165 (1960).
- <sup>17</sup>N. V. Zavaritskiĭ and V. N. Zavaritskiĭ, *Zh. Eksp. Teor. Fiz.* **83**, 1182 (1982) [*Sov. Phys. JETP* **56**, 674 (1982)].
- <sup>18</sup>L. J. Sham, J. S. Allen, Jr., A. Kamger, and D. C. Tsui, *Phys. Rev. Lett.* **40**, 472 (1978).
- <sup>19</sup>W. Sesselman and J. P. Kotthaus, *Solid State Commun.* **39**, 193 (1979).

Translated by Dave Parsons